

Non-linear magnons in the 1/3 magnetization plateau of a proximate quantum spin liquid

A. O. Scheie,^{1,*} Y. Kamiya,² Hao Zhang,³ Sangyun Lee,⁴ A.J. Woods,⁴ M. G. Gonzalez,⁵ B. Bernu,⁵ J. Xing,⁶ D. M. Pajerowski,¹ Haidong Zhou,³ A. S. Sefat,⁶ L. Messio,^{5,7} R. Movshovich,⁴ C. D. Batista,^{3,8} and D. A. Tennant^{3,8,9}

¹Neutron Scattering Division, Oak Ridge National Laboratory, Oak Ridge, TN 37831, USA

²School of Physics and Astronomy, Shanghai Jiao Tong University 800 Dongchuan Road, Minhang District, Shanghai 200240, China

³Department of Physics and Astronomy, University of Tennessee, Knoxville, TN 37996, USA

⁴MPA-Q, Los Alamos National Laboratory, Los Alamos, New Mexico 87545, USA

⁵Sorbonne Université, CNRS, Laboratoire de Physique Théorique de la Matière Condensée, LPTMC, F-75005 Paris, France

⁶Materials Science and Technology Division, Oak Ridge National Laboratory, Oak Ridge, Tennessee 37831, USA

⁷Institut Universitaire de France (IUF), F-75005 Paris, France

⁸Shull Wollan Center, Oak Ridge National Laboratory, TN 37831, USA

⁹Quantum Science Center, Oak Ridge National Laboratory, TN 37831, USA

(Dated: August 1, 2022)

Quantum spin liquids (QSL) are theoretical states of matter with long-range entanglement and exotic quasiparticles. However, they elude quantitative theory, rendering their underlying phases mysterious, and hampering experimental efforts to determine candidate materials' interactions. Here we study resonating valence bond QSL candidate material KYbSe₂ in its 1/3 plateau phase, where quantitative theory is tractable. We measure the magnon modes within this phase using inelastic neutron scattering and fit them using nonlinear spin wave theory, and we also fit the heat capacity using high temperature series expansion. Both fits yield the same magnetic Hamiltonian to within uncertainty, confirming previous estimates and showing the Heisenberg J_2/J_1 to be an accurate model for KYbSe₂, and confirming its status as a proximate QSL.

Triangular lattice quantum magnets have been of intense interest since Anderson's 1973 prediction of a resonating valence bond (RVB) quantum spin liquid (QSL) [1], but no clear triangular QSL materials exist [2]. In this state, antiferromagnetic interacting spins on a two-dimensional triangular lattice produce a long-range entangled quantum spin liquid rather than conventional long range order [3]. This state has intriguing theoretical properties [4], and quantum spin liquids holds great potential for quantum electronic technologies [5, 6]. Although Anderson's original proposal was for the nearest neighbor Heisenberg antiferromagnet, subsequent studies showed the pure nearest neighbor model actually orders into a 120° phase at the lowest temperatures [7, 8]. Instead, the QSL state requires a small second neighbor J_2 exchange between $\approx 6\%$ and $\approx 16\%$ of the nearest neighbor exchange to stabilize [9–15]. (A similar role is played by nearest neighbor anisotropic exchange [16].) Although it is unclear whether this J_2 -stabilized phase is Anderson's RVB or a different type of QSL [15, 17], it is clear that the QSL state should exist—if a material with the right Hamiltonian could be found.

Many materials have been proposed as 2D triangular lattice antiferromagnets, including Ba₃CoSb₂O₉ [18–20], YbMgGaO₄ [21–25], and organic salts [26–28]. However, none of these have been found to have an RVB ground state. A promising new class of materials is the Yb³⁺ delafossites, which have magnetic Yb³⁺ in a crystallographically perfect 2D triangular lattice [3, 29–32, 34]. However, the crucial test in evaluating candidate RVB materials is whether their magnetic exchange Hamiltonians are indeed within a theoretical QSL phase.

Part of the difficulty in experimentally studying an RVB liquid is that it lacks sharp spectral features: its elementary

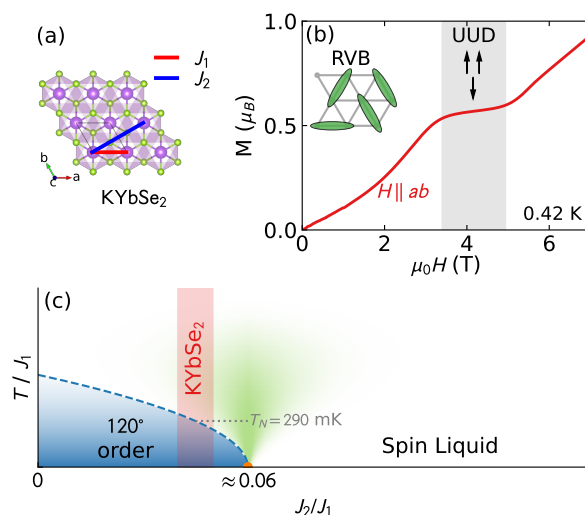


FIG. 1. KYbSe₂ crystal structure and phase diagram. (a) The triangular lattice plane with the J_1 and J_2 exchanges between magnetic Yb sites. (b) The 0.42 K in-plane magnetization from Ref. [3], showing a 1/3 magnetization plateau phase at 4 T. (c) The J_2/J_1 phase diagram, showing the refined KYbSe₂ J_2/J_1 is extremely close to the resonating valence bond (RVB) spin liquid state.

quasiparticles are $S = 1/2$ spinons, which are created in pairs and thus produce a diffuse continuum [35, 36]. And unfortunately, diffuse continua are also produced by disordered or glassy states and are thus ambiguous [25, 37]. However, an important feature of the quantum $S = 1/2$ triangular lattice antiferromagnet is that an applied magnetic field produces a 1/3-magnetization plateau phase corresponding to up-up-down long range magnetic order [38, 39]. This is an inherently quantum mechanical effect, whereby quantum fluctuations select a collinear spin ordering [40]. Crucially, this produces

* scheieao@ornl.gov

well-defined magnon modes within the plateau phase, whose gapped dispersion can be calculated via nonlinear spin wave theory [6, 40]. This observation allows us to extract the Hamiltonian parameters without the need for reaching the fully polarized magnetic state (the saturation field is prohibitively large for most RVB candidate materials [6, 42]). The problem thus becomes tractable by studying the magnons in the plateau phase.

KYbSe₂ [3] was recently studied using neutron scattering, and fits to paramagnetic diffuse scattering show it to be a proximate QSL: it orders magnetically at 290 mK, but its fitted J_2/J_1 ratio is close enough to the QSL phase to exhibit some of its exotic behaviors (see Fig. 1), including diffuse zero-field neutron spectra from bound spinons [2]. However, the previous fit relied upon classical models compared to paramagnetic scattering. A robust Hamiltonian fit requires quantum calculations. Here we provide such analysis using inelastic magnetic scattering and heat capacity, showing KYbSe₂ to be a remarkably good realization of the J_2/J_1 triangular lattice Heisenberg antiferromagnet.

Like the ideal 2D triangular Heisenberg model [38, 39], KYbSe₂ has a 1/3 saturation magnetization plateau at an in-plane magnetic field of 4 T [Fig. 1(b)], which also accompanies a reentrant magnetic ordered phase [3]. Presumably, this ordered phase is the up-up-down phase of the quantum $S = 1/2$ triangular lattice antiferromagnet. This finite field ordered phase is itself evidence of a highly quantum ground state, and also provides an opportunity to observe coherent spin wave modes at modest magnetic field, and fit them to a non-linear spin wave theory (NLSWT).

We measured the KYbSe₂ scattering in the hhl scattering plane using the CNCS spectrometer [44] at Oak Ridge National Laboratory's Spallation Neutron Source [45]. The sample was mounted in a dilution refrigerator and oriented with the $[1\bar{1}0]$ direction along a vertical magnetic field. The scattering was measured at applied fields of 0 T, 4 T, and 8 T at a 100 mK base temperature, with a 12 K zero field data set collected and subtracted as background (see Supplemental Information for details [46]). The data are shown in Fig. 2.

The zero field neutron scattering in Fig. 2 shows a diffuse continuum with a sharp lower bound becoming gapless at $(1/3, 1/3, 0)$ as reported previously [2]. When the magnetic field is set to within the plateau field (4 T), well-defined spin wave modes appear, similar to what was reported in CsYbSe₂ [5]. When the magnetic field is increased further beyond the plateau field, the well-defined modes disappear, replaced again by broad, diffuse features—although there are sharply defined features at $hh = (0, 0)$ and $(1/3, 1/3)$ at 8 T as shown in Fig. 2(i)-(l). At all fields, there is no detectable dispersion in the ℓ direction (right columns of Fig. 2), signaling highly two-dimensional magnetism and very weak interplane exchange. However, at 4 T there is noticeable intensity modulation in the modes, as shown in Fig. 2(g). This signals nonzero interplane correlations. However, the elastic scattering shows that these correlations do not extend beyond one neighboring triangular plane (see Supplemental Information [46]).

The well defined modes at 4 T provide an opportunity to fit the magnetic exchange Hamiltonian using nonlinear spin wave

theory (NLSWT) [6, 40]. This provides an independent test of whether the J_1 - J_2 Hamiltonian is appropriate to KYbSe₂, and what the J_2/J_1 ratio is.

We assume a J_1 - J_2 Hamiltonian in a magnetic field

$$\hat{\mathcal{H}} = J_1 \sum_{\langle i,j \rangle} \hat{S}_i \cdot \hat{S}_j + J_2 \sum_{\langle\langle i,j \rangle\rangle} \hat{S}_i \cdot \hat{S}_j - h \sum_i \hat{S}_i^x \quad (1)$$

where $h = g_{xx}\mu_B B$, B is the magnitude of the applied magnetic field along the x -direction and $g_{\alpha\beta}$ is the g -tensor.

By following the procedure described in Ref. [6], we fit the NLSWT magnon dispersion to the mode energies as a function of wavevector extracted from Gaussian profiles at constant Q slices [see Fig. 3(a)]. Treating the three Hamiltonian parameters J_1 , J_2 , and h as fitted constants (magnetic field h is a fitted parameter because g_{xx} has large uncertainty for KYbSe₂ [48]), we fit the NLSWT mode energies to the experimentally measured dispersions as shown in Fig. 3(c). This gives a very good reproduction of the lower energy modes, as shown in Fig. 3(b). To define uncertainty, we calculated a contour $\Delta\chi^2_{\text{red}} = 1$ above the reduced χ^2 minimum [49]. One standard deviation and two standard deviation contours are plotted in Fig. 3(d). Using a one standard deviation uncertainty, the best fit values are $J_1 = (0.456 \pm 0.013)$ meV, $J_2/J_1 = 0.043 \pm 0.010$, and $h/J_1 = 1.73 \pm 0.05$. This J_2/J_1 ratio agrees to within uncertainty with the $J_2/J_1 = 0.047 \pm 0.007$ from the Onsager reaction field fits in Ref. [2]. We note that the exact saturation field for the proposed model is $h_{\text{sat}}/J_1 = 9/2$, implying that $h/h_{\text{sat}} = 0.38 \pm 0.01$.

Single-magnon NLSWT calculations did not capture the dispersive feature above 1 meV in Fig. 3(a). However, two-magnon continuum calculations (shown in the Supplemental Information [46]) do capture this feature. The sharpness of this mode in an otherwise diffuse continuum arises from the two-dimensional nature of the system, such that the density of two-magnon states has a Van Hove singularities at an energies that depend on their total momentum. These singularities are broadened by the finite experimental resolution, leading to a dispersive peak in the continuum scattering arising from the longitudinal spin structure factor, as was seen in YbCl₃ [50].

As another independent test of our J_2/J_1 model, we also compared the KYbSe₂ heat capacity to theoretical calculations. Using the zero field heat capacity reported in Refs. [2, 3], subtracted by KLuSe₂ heat capacity to isolate the magnetic heat capacity (see the Supplemental Information for details [46]), we compared the data to the high temperature series expansion interpolation calculations [51–54], which give accurate quantum calculations of the high temperature heat capacity of the 2D triangular lattice as a function of J_2/J_1 . The series were calculated out to the 14th order (one order more than Ref. [54]). These data are shown in Fig. 4.

The zero field heat capacity was measured in a dilution refrigerator below 2.5 K and a ⁴He cryostat above 1.8 K separately and combined. For temperatures greater than 2 K, the theory and experiment match very closely, with subtle differences depending on the precise J_2/J_1 value. To quantitatively compare theory and experiment, we define a χ^2_{red} for $2 \text{ K} < T < 8 \text{ K}$. (8 K is where the lattice heat capacity becomes much larger than the magnetic contribution, and the

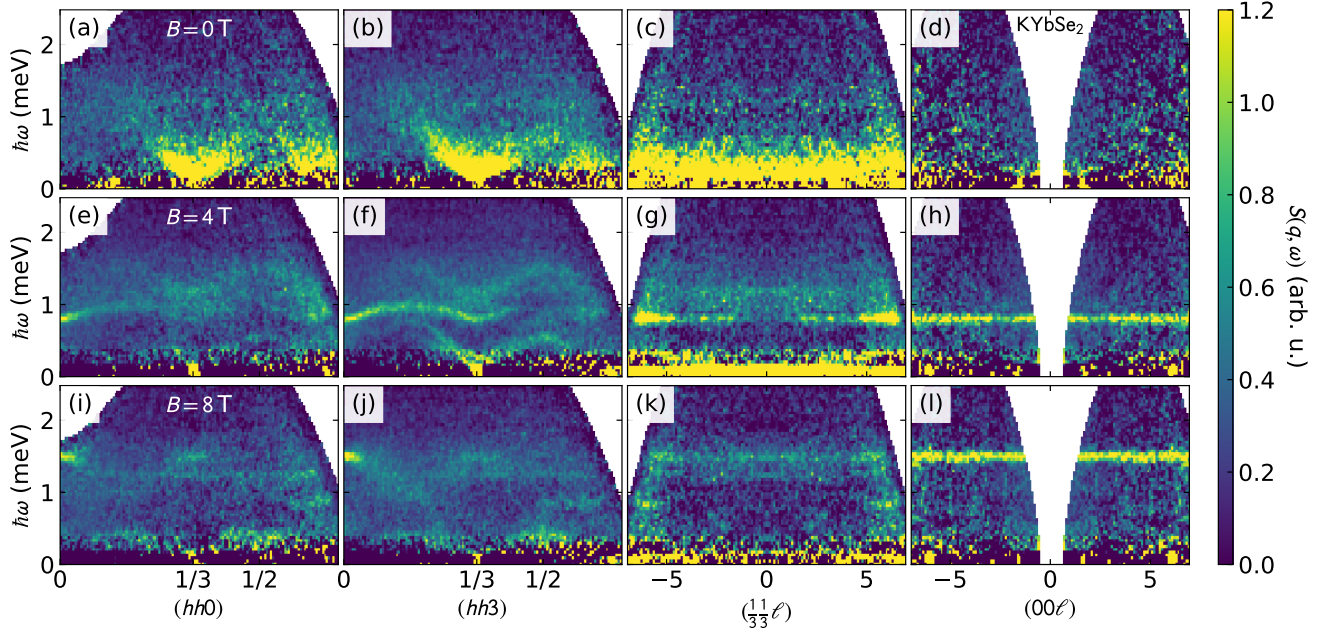


FIG. 2. KYbSe₂ field dependent scattering. The top row shows the zero field neutron spectrum, showing a diffuse continuum with a lower bound coming to zero energy at $hh = (1/3, 1/3)$ (in reciprocal lattice units). The middle row shows the same slices for $B = 4$ T and the bottom row for $B = 8$ T. The left two columns show cuts along hh (the far left integrated over $-1.5 < \ell < 1.5$ r.l.u., the center-left column integrated over $1.5 < \ell < 4.5$), and the right two columns show cuts along ℓ . For $B = 0$ T and $B = 8$ T, there is no appreciable ℓ dependence to the scattering, but at $B = 4$ T there is a modulated intensity to some of the features as shown most clearly in panel (g).

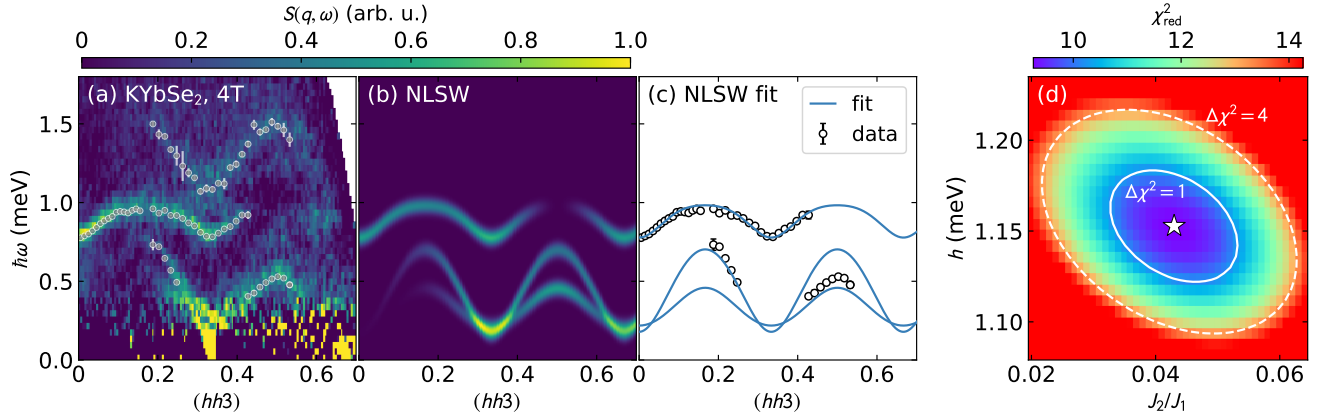


FIG. 3. Nonlinear spin wave fit to KYbSe₂ scattering at 4 T. The left panel shows the experimental scattering integrated along $(hh3)$, with the grey data points indicating the mode centers determined using constant Q cuts fitted to a Gaussian profile in energy. Panel (b) shows the best calculated neutron spectrum from nonlinear spin wave theory (NLSWT). Note that the highest energy mode is not captured by the single-magnon scattering calculation. Panel (c) shows the fitted points from panel (a) with the NLSWT dispersion curves used to fit the data. Panel (d) shows the one and two standard deviation χ^2 contours of J_2/J_1 and magnetic field h .

subtracted values are more questionable.) For each theoretical J_2/J_1 value, we fit J_1 to minimize χ^2 and thus obtain χ^2_{red} as a function of J_2/J_1 , shown as an inset to Fig. 4. This fit yields best fit values of $J_1 = (0.439 \pm 0.010)$ meV and $J_2/J_1 = 0.037 \pm 0.013$. This agrees to within uncertainty with the results from NLSWT fits.

It should be noted that the high temperature expansion does not capture either the maximum in heat capacity at 1 K or the ordering transition at 290 mK. The lack of ordering tran-

sition is not surprising as the theory is based off a perfectly isotropic 2D lattice, which only orders at $T = 0$ [55]. The 1 K “bump”, also seen in NaYbO₂ [31], is more challenging to explain. The failure of the high-temperature expansion in capturing this peak suggests that it is either induced by an increase of the magnetic in-plane correlation length beyond several lattice spaces, $\xi \gtrsim 10a$, or by the onset of three-dimensional correlations in KYbSe₂, which ultimately leads to long range magnetic order. Be that as it may, the series expansion theory

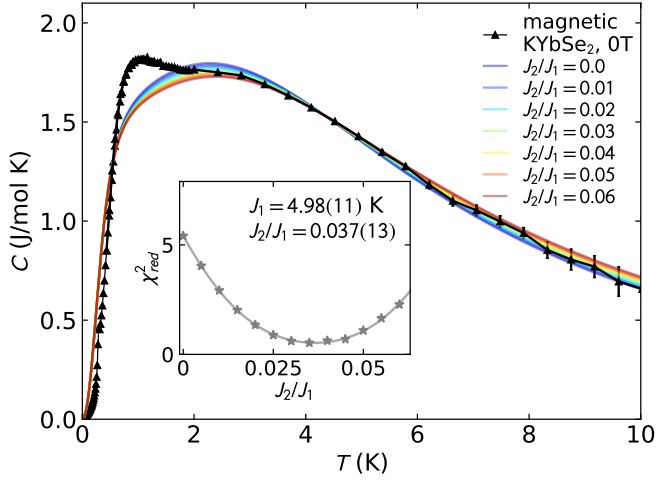


FIG. 4. KYbSe₂ zero-field heat capacity (black) compared to theoretical calculations of the heat capacity from Ref. [54]. For the theory, the only adjustable parameter is the T axis scaling (corresponding to J_1). The inset shows reduced χ^2 as a function of J_2/J_1 , showing a minimum at $J_2/J_1 = 0.040(12)$.

TABLE I. Best fit exchange Hamiltonian value for KYbSe₂ from three different experiments and three different theoretical techniques. Note that the Onsager reaction field theory from Ref. [2] cannot estimate J_1 as it is classical. The last row gives the weighted mean.

Theoretical technique	J_1 (meV)	J_2/J_1
Onsager reaction field	NA	0.047 ± 0.007
Nonlinear spin waves	0.456 ± 0.013	0.043 ± 0.010
Heat capacity	0.429 ± 0.010	0.037 ± 0.013
Weighted mean:	0.438 ± 0.008	0.044 ± 0.005

gives an excellent description of the > 2 K heat capacity, and allows us to extract both J_1 and J_2 from the data.

At this point, we have three independent fits of the KYbSe₂ magnetic exchange Hamiltonian, which are summarized in Table I. Each fit used a different experiment and a different experimental technique, so it is remarkable that all three agree to within uncertainty. The two theoretical fits performed in this study (NLSWT and high temperature heat capacity series expansion) include quantum effects, and are appropriate for the highly quantum KYbSe₂. That being said, the Onsager reaction field theory fit agrees to within uncertainty with these two

other methods even though it neglects quantum effects. This is evidence that fitting paramagnetic scattering with classical methods [56] works even for highly quantum systems. Also, this is a remarkable confirmation of the results and methodology in Ref. [2].

The study here shows that KYbSe₂ is an excellent example of a spin-1/2 J_2/J_1 Heisenberg magnet on a triangular lattice. The use of nonlinear spin-wave theory at an intermediate—rather than fully saturated—field provides an alternative method to that in Ref. [42] which requires a fully polarized system. This is then applicable not only to other delafossite materials but also other candidate spin liquids where the saturation field cannot be reached. The confirmation that KYbSe₂ is very close to a quantum spin liquid state provides strong impetus to further study this class of compounds as a rational route to quantum spin liquids.

In conclusion, we have used two quantum simulation techniques to fit the KYbSe₂ magnetic exchange Hamiltonian to experimental data: nonlinear spin waves to finite-field scattering in a plateau phase, and high temperature expansions to zero field heat capacity. Both give extremely good agreement with experiment (down to an energy scale of 2 K), showing that the Heisenberg J_2/J_1 model is an excellent minimal model for KYbSe₂. Furthermore, we find a J_2/J_1 ratio extremely close to the 2D triangular lattice spin liquid state at $J_2/J_1 \approx 0.06$. With three independent experimental measurements all giving the same result, this definitively verifies the model proposed in Ref. [2]. Thus we expect to find approximate spin liquid behavior in KYbSe₂ and in related materials.

Acknowledgments

This research used resources at the Spallation Neutron Source, a DOE Office of Science User Facility operated by the Oak Ridge National Laboratory. The work by D.A. Tennant is supported by the Quantum Science Center (QSC), a National Quantum Information Science Research Center of the U.S. Department of Energy (DOE). J. Xing and A. Sefat were supported by U.S. Department of Energy, Basic Energy Sciences, Materials Science and Engineering Division. H.Z. was supported by the U.S. Department of Energy under Grant No. DE-SC0020254. S.L., A.W., and R.M. were supported by the U.S. Department of Energy, Office of Science, National Quantum Information Science Research Centers, and Quantum Science Center.

[1] P. Anderson, *Materials Research Bulletin* **8**, 153 (1973).
[2] C. Broholm, R. J. Cava, S. A. Kivelson, D. G. Nocera, M. R. Norman, and T. Senthil, *Science* **367** (2020), 10.1126/science.aay0668.
[3] L. Balents, *Nature* **464**, 199 (2010).
[4] Y. Zhou, K. Kanoda, and T.-K. Ng, *Rev. Mod. Phys.* **89**, 025003 (2017).

[5] C. Nayak, S. H. Simon, A. Stern, M. Freedman, and S. Das Sarma, *Rev. Mod. Phys.* **80**, 1083 (2008).
[6] Y. Tokura, M. Kawasaki, and N. Nagaosa, *Nature Physics* **13**, 1056 (2017).
[7] L. Capriotti, A. E. Trumper, and S. Sorella, *Phys. Rev. Lett.* **82**, 3899 (1999).
[8] S. R. White and A. L. Chernyshev, *Phys. Rev. Lett.* **99**, 127004 (2007).

- [9] Z. Zhu and S. R. White, *Phys. Rev. B* **92**, 041105 (2015).
- [10] W.-J. Hu, S.-S. Gong, W. Zhu, and D. N. Sheng, *Phys. Rev. B* **92**, 140403 (2015).
- [11] Y. Iqbal, W.-J. Hu, R. Thomale, D. Poilblanc, and F. Becca, *Phys. Rev. B* **93**, 144411 (2016).
- [12] S. N. Saadatmand and I. P. McCulloch, *Phys. Rev. B* **94**, 121111 (2016).
- [13] A. Wietek and A. M. Läuchli, *Phys. Rev. B* **95**, 035141 (2017).
- [14] S.-S. Gong, W. Zhu, J.-X. Zhu, D. N. Sheng, and K. Yang, *Phys. Rev. B* **96**, 075116 (2017).
- [15] S. Hu, W. Zhu, S. Eggert, and Y.-C. He, *Phys. Rev. Lett.* **123**, 207203 (2019).
- [16] Z. Zhu, P. A. Maksimov, S. R. White, and A. L. Chernyshev, *Phys. Rev. Lett.* **120**, 207203 (2018).
- [17] S.-S. Gong, W. Zheng, M. Lee, Y.-M. Lu, and D. N. Sheng, *Phys. Rev. B* **100**, 241111 (2019).
- [18] S. Ito, N. Kurita, H. Tanaka, S. Ohira-Kawamura, K. Nakajima, S. Itoh, K. Kuwahara, and K. Kakurai, *Nature Communications* **8**, 235 (2017).
- [19] D. Macdougall, S. Williams, D. Prabhakaran, R. I. Bewley, D. J. Voneshen, and R. Coldea, *Phys. Rev. B* **102**, 064421 (2020).
- [20] J. Ma, Y. Kamiya, T. Hong, H. B. Cao, G. Ehlers, W. Tian, C. D. Batista, Z. L. Dun, H. D. Zhou, and M. Matsuda, *Phys. Rev. Lett.* **116**, 087201 (2016).
- [21] Y. Li, G. Chen, W. Tong, L. Pi, J. Liu, Z. Yang, X. Wang, and Q. Zhang, *Phys. Rev. Lett.* **115**, 167203 (2015).
- [22] Y. Shen, Y.-D. Li, H. Wo, Y. Li, S. Shen, B. Pan, Q. Wang, H. C. Walker, P. Steffens, M. Boehm, Y. Hao, D. L. Quintero-Castro, L. W. Harriger, M. D. Frontzek, L. Hao, S. Meng, Q. Zhang, G. Chen, and J. Zhao, *Nature* **540**, 559 (2016).
- [23] J. A. M. Paddison, M. Daum, Z. Dun, G. Ehlers, Y. Liu, M. Stone, H. Zhou, and M. Mourigal, *Nature Physics* **13**, 117 (2017).
- [24] Y. Xu, J. Zhang, Y. S. Li, Y. J. Yu, X. C. Hong, Q. M. Zhang, and S. Y. Li, *Phys. Rev. Lett.* **117**, 267202 (2016).
- [25] Z. Zhu, P. A. Maksimov, S. R. White, and A. L. Chernyshev, *Phys. Rev. Lett.* **119**, 157201 (2017).
- [26] T. Itou, A. Oyamada, S. Maegawa, M. Tamura, and R. Kato, *Phys. Rev. B* **77**, 104413 (2008).
- [27] S. Yamashita, Y. Nakazawa, M. Oguni, Y. Oshima, H. Nojiri, Y. Shimizu, K. Miyagawa, and K. Kanoda, *Nature Physics* **4**, 459 (2008).
- [28] K. Riedl, R. Valentí, and S. M. Winter, *Nature Communications* **10**, 2561 (2019).
- [29] L. Ding, P. Manuel, S. Bachus, F. Grußler, P. Gegenwart, J. Singleton, R. D. Johnson, H. C. Walker, D. T. Adroja, A. D. Hillier, and A. A. Tsirlin, *Phys. Rev. B* **100**, 144432 (2019).
- [30] M. Baenitz, P. Schlender, J. Sichelschmidt, Y. A. Onykiienko, Z. Zangeneh, K. M. Ranjith, R. Sarkar, L. Hozoi, H. C. Walker, J.-C. Orain, H. Yasuoka, J. van den Brink, H. H. Klauss, D. S. Inosov, and T. Doert, *Phys. Rev. B* **98**, 220409 (2018).
- [31] M. M. Bordelon, E. Kenney, C. Liu, T. Hogan, L. Posthuma, M. Kavand, Y. Lyu, M. Sherwin, N. P. Butch, C. Brown, M. J. Graf, L. Balents, and S. D. Wilson, *Nature Physics* **15**, 1058 (2019).
- [32] R. Sarkar, P. Schlender, V. Grinenko, E. Haeussler, P. J. Baker, T. Doert, and H.-H. Klauss, *Phys. Rev. B* **100**, 241116 (2019).
- [33] J. Xing, L. D. Sanjeewa, A. F. May, and A. S. Sefat, *APL Materials* **9**, 111104 (2021).
- [34] P.-L. Dai, G. Zhang, Y. Xie, C. Duan, Y. Gao, Z. Zhu, E. Feng, Z. Tao, C.-L. Huang, H. Cao, A. Podlesnyak, G. E. Granroth, M. S. Everett, J. C. Neuefeind, D. Voneshen, S. Wang, G. Tan, E. Morosan, X. Wang, H.-Q. Lin, L. Shu, G. Chen, Y. Guo, X. Lu, and P. Dai, *Phys. Rev. X* **11**, 021044 (2021).
- [35] S. A. Kivelson, D. S. Rokhsar, and J. P. Sethna, *Phys. Rev. B* **35**, 8865 (1987).
- [36] P. W. Anderson, G. Baskaran, Z. Zou, and T. Hsu, *Phys. Rev. Lett.* **58**, 2790 (1987).
- [37] I. Kimchi, A. Nahum, and T. Senthil, *Phys. Rev. X* **8**, 031028 (2018).
- [38] H. Nishimori and S. Miyashita, *Journal of the Physical Society of Japan* **55**, 4448 (1986).
- [39] A. V. Chubukov and D. I. Golosov, *Journal of Physics: Condensed Matter* **3**, 69 (1991).
- [40] J. Alicea, A. V. Chubukov, and O. A. Starykh, *Phys. Rev. Lett.* **102**, 137201 (2009).
- [6] Y. Kamiya, L. Ge, T. Hong, Y. Qiu, D. L. Quintero-Castro, Z. Lu, H. B. Cao, M. Matsuda, E. S. Choi, C. D. Batista, M. Mourigal, H. D. Zhou, and J. Ma, *Nature Communications* **9**, 2666 (2018).
- [42] R. Coldea, D. A. Tennant, K. Habicht, P. Smeibidl, C. Wolters, and Z. Tylczynski, *Phys. Rev. Lett.* **88**, 137203 (2002).
- [2] A. Scheie, E. Ghioldi, J. Xing, J. Paddison, N. Sherman, M. Dupont, D. Abernathy, D. Pajerowski, S.-S. Zhang, L. Manuel, *et al.*, *arXiv preprint arXiv:2109.11527* (2021).
- [44] G. Ehlers, A. A. Podlesnyak, J. L. Niedziela, E. B. Iverson, and P. E. Sokol, *Review of Scientific Instruments* **82**, 085108 (2011).
- [45] T. E. Mason, D. Abernathy, I. Anderson, J. Ankner, T. Egami, G. Ehlers, A. Ekkebus, G. Granroth, M. Hagen, K. Herwig, J. Hodges, C. Hoffmann, C. Horak, L. Horton, F. Klose, J. Larese, A. Mesecar, D. Myles, J. Neuefeind, M. Ohl, C. Tulk, X.-L. Wang, and J. Zhao, *Physica B: Condensed Matter* **385**, 955 (2006).
- [46] See Supplemental Material at [URL will be inserted by publisher] for more details of the experiments and calculations.
- [5] T. Xie, J. Xing, S. Nikitin, S. Nishimoto, M. Brando, P. Khanenko, J. Sichelschmidt, L. Sanjeewa, A. S. Sefat, and A. Podlesnyak, *arXiv preprint arXiv:2106.12451* (2021).
- [48] A. Scheie, P. Laurell, A. M. Samarakoon, B. Lake, S. E. Nagler, G. E. Granroth, S. Okamoto, G. Alvarez, and D. A. Tennant, *Phys. Rev. B* **103**, 224434 (2021).
- [49] W. H. Press, S. A. Teukolsky, W. T. Vetterling, and B. P. Flannery, *Numerical recipes 3rd edition: The art of scientific computing* (Cambridge university press, 2007).
- [50] G. Sala, M. B. Stone, B. K. Rai, A. F. May, P. Laurell, V. O. Garlea, N. P. Butch, M. D. Lumsden, G. Ehlers, G. Pokharel, *et al.*, *Nature communications* **12**, 1 (2021).
- [51] B. Bernu and G. Misguich, *Phys. Rev. B* **63**, 134409 (2001).
- [52] H.-J. Schmidt, A. Hauser, A. Lohmann, and J. Richter, *Phys. Rev. E* **95**, 042110 (2017).
- [53] B. Bernu, L. Pierre, K. Essafi, and L. Messio, *Phys. Rev. B* **101**, 140403 (2020).
- [54] M. G. Gonzalez, B. Bernu, L. Pierre, and L. Messio, *SciPost Phys.* **12**, 112 (2022).
- [55] N. D. Mermin and H. Wagner, *Phys. Rev. Lett.* **17**, 1133 (1966).
- [56] J. A. M. Paddison, *Phys. Rev. Lett.* **125**, 247202 (2020).

SUPPLEMENTAL INFORMATION FOR NON-LINEAR MAGNONS IN THE 1/3 MAGNETIZATION PLATEAU OF A PROXIMATE QUANTUM SPIN LIQUID

I. EXPERIMENTS

A. Cold Neutron Chopper Spectrometer (CNCS)

For the CNCS experiment, we used a sample made of 19 coaligned crystals (total mass ~ 200 mg) oriented in the (hhl) scattering plane glued to aluminum plates (see Fig. S1). The sample was mounted in a helium dilution refrigerator with an 8 T magnet and measured with double-disc chopper frequency 300.0 Hz (high-flux mode, 9 degree opening on the double disk) for an incident energy $E_i = 3.32$ meV. At each field the sample was rotated 180° to map the neutron spectrum. The processed CNCS data was then corrected for the isotropic Yb^{3+} form factor [S1]. This data (prior to background subtraction) is shown in Fig. S2. The left two columns are integrated over $\ell \pm 1.5$ reciprocal lattice units (RLU), and the right two columns are integrated over $hh \pm 0.02$ RLU, and the integration ranges for the main text data are the same.



FIG. S1. KYbSe_2 sample used to measure the field-dependent spin excitations on CNCS. 19 plate-like crystals were coaligned and glued to two aluminum plates with the $[1\bar{1}0]$ direction vertical and the $[001]$ direction orthogonal to the aluminum surface.

To clearly resolve the low-energy magnetic scattering, it was necessary to subtract the background (sample environment scattering and phonon scattering) from the data. Because a perfect background is not available for this data, we created a phenomenological background using 12 K scattering data where magnetic correlations are negligible [S2, S3], shown in Fig. S3(a)-(d). Because the higher temperature intensifies phonon scattering, we removed certain intense inelastic features in the slices and filled in via Astropy's interpolation routine [S4]. Then, following the method in Ref. [S2], we subtracted the median intensity for each energy from the scattering data for inelastic (> 0.38 meV) data. Finally, we convolved the inelastic (> 0.38 meV) data with a two-dimensional Gaussian profile to reduce the noise. This final phenomenological background is shown in Fig. S3(e)-(f). By comparing the supplemental information Fig. S2 to the main text Fig. 1, it is clear that this approach approximately isolates the magnetic

scattering quite nicely.

Although the data have a large elastic background, substantial elastic scattering appears in the finite-field plateau phase, plotted in Fig. S4. At 4 T, a streak of scattering appears at $(1/3, 1/3, \ell)$, in accord with in-plane magnetic order of the plateau phase. If we isolate the magnetic scattering by subtracting the 0 T data (where the magnetic order is extremely weak and barely any elastic magnetic signal is visible) from the 4 T data as in Fig. S4(e), we see that the 4 T magnetic signal has a sinusoidal intensity modulation with ℓ , as shown in Fig. S4(f). The intensity peaks at $\ell = 0$ and $\ell = \pm 3$, the same periodicity as the triangular planes, signaling short-ranged ferromagnetic correlations between the triangular lattice planes with a propagation vector $Q = (1/3, 1/3, 0)$. This is markedly different from the elastic magnetic scattering at 4 T measured in CsYbSe_2 , which had maximal intensity at $\ell = \pm 1$ and a propagation vector $Q = (1/3, 1/3, 1)$ [S5]. Furthermore, in CsYbSe_2 the correlations extend to at least three triangular lattice planes, but in KYbSe_2 the magnetic correlations appear to extend only to the neighboring planes. Thus KYbSe_2 appears to be more two-dimensional than CsYbSe_2 .

B. Heat capacity uncertainty

The heat capacity data presented in the main text is made of two different measurements: one measured in a dilution refrigerator [S2], and another on a Quantum Design PPMS with a ^3He insert [S3]. The KYbSe_2 sample mass was measured more precisely for the dilution refrigerator experiment, and thus we scaled the higher temperature PPMS data to match the dilution refrigerator measurement for the temperature window $0.4 \text{ K} < T < 2.0 \text{ K}$, giving a renormalizing scale factor of 0.99 to the high temperature data. Heat capacity of nonmagnetic KLuSe_2 was subtracted from all data to isolate the magnetic heat capacity.

The uncertainties for the heat capacity values came from three sources: (i) uncertainty in mass normalization, which we estimate from the difference between the absolute heat capacities of the two different dilution refrigerator measurements on two different KYbSe_2 samples reported in Ref. [S2]. (ii) Variance in heat capacity measured at the same temperature: in the ^3He heat capacity measurement, data points were repeated three times at each temperature. (iii) Difference in heat capacity between two separate ^3He refrigerator measurements. The uncertainties from these three sources were added in quadrature to yield the uncertainties plotted in the main text Fig. 4.

II. NONLINEAR SPIN WAVES

A. Two magnon continuum

In the experimental KYbSe_2 scattering, an additional broadened mode is visible above 1 meV which is not captured by the single-magnon NLSWT calculation (main text Fig. 3). However, when we calculate the two-magnon continuum scattering

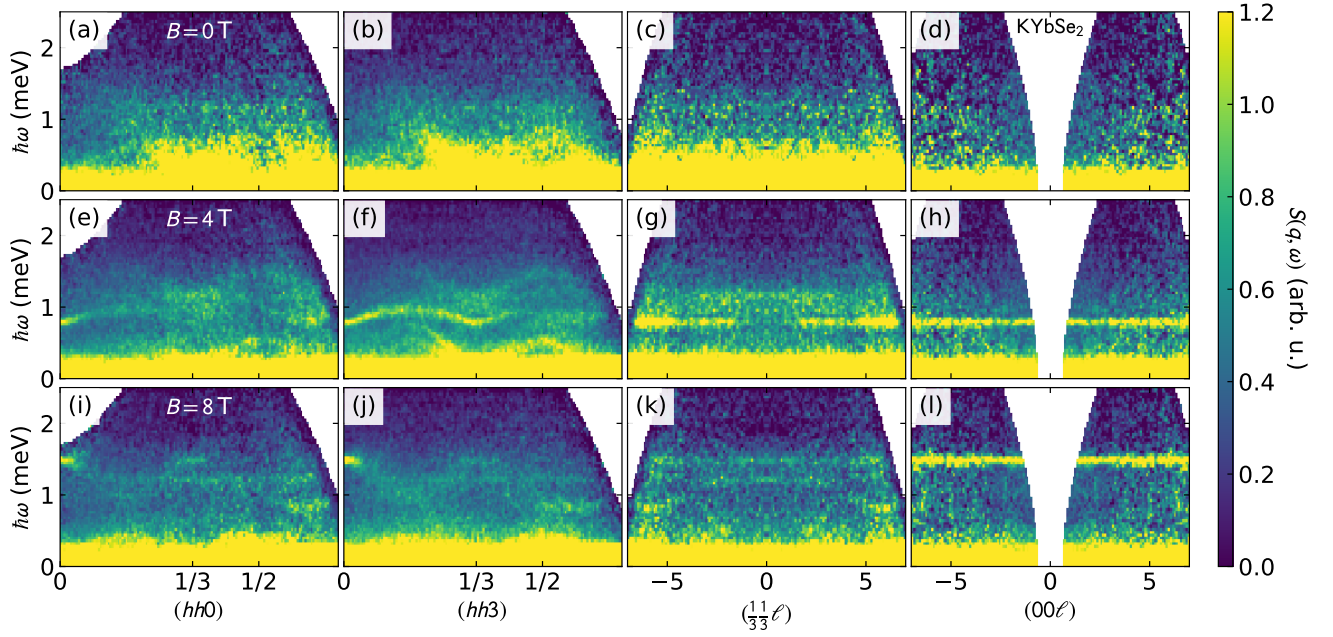


FIG. S2. KYbSe₂ field dependent scattering without background subtraction. The top row shows the zero field neutron spectrum, the middle row shows the same slices for $B = 4$ T, and the bottom row for $B = 8$ T. These data should be compared with main text Fig. 1. At high energy transfers the features are clear, but background subtraction (Fig. S3) is necessary to resolve low energy features.

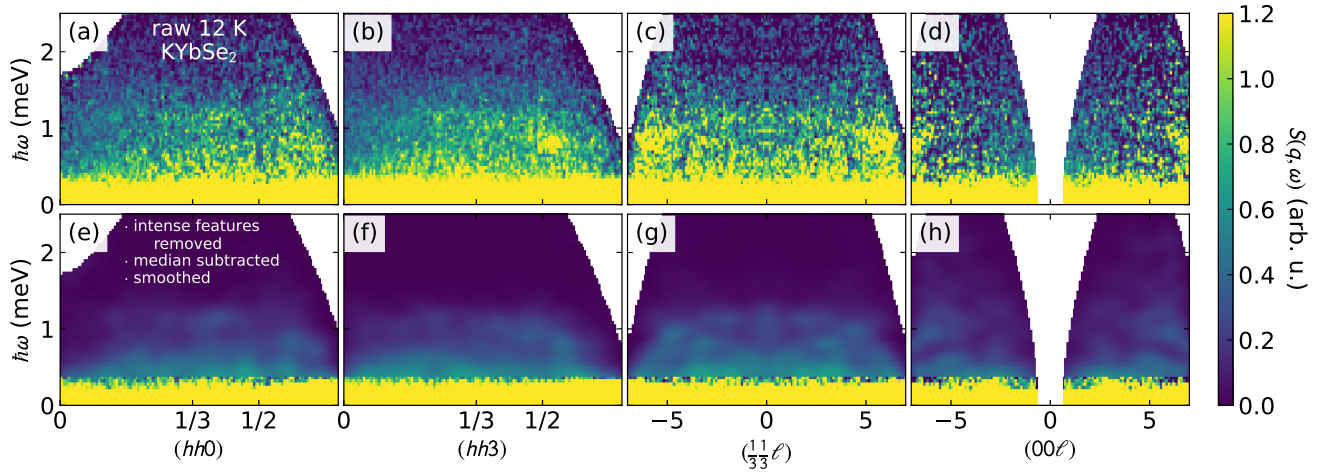


FIG. S3. KYbSe₂ scattering background. The top row shows the raw $T = 12$ K data. To process this and use it as a background for the data in Fig. S2, we removed the intense features [e.g., at 0.7 meV in panel (b)], subtracted the energy-dependent median inelastic scattering intensity from every energy, and convolved with a Gaussian function to smooth the data. This resulted in the background in the bottom row, which was subtracted from the scattering data in Fig. S2 to generate the data in main text Fig 1.

(following the method in Ref. [S6]), we see a similar mode appear in the simulation, as shown Fig. S5(b).

Although the overall character and bandwidth of the calculated two-magnon continuum matches experiment, Fig. S5(c) shows the calculated intensity is slightly weaker than what is experimentally observed. There could be several explanations for this: (i) the experimental background subtraction was imperfect and left some nonlinear anomalous intensity above 1 meV. (ii) The g -tensor is different than the best fit crystal field values (g_{zz} has a very large error bar [S2]), which leads

to different weight being given to S_{xx} vs S_{yy} and S_{zz} and more intensity in the continuum. (iii) The NLSWT approximation neglects higher order effects, and thus it may be slightly underestimating the weight of the continuum scattering. Despite this discrepancy, because of the close resemblance to the experimental dispersion, we are confident that the observed mode above 1 meV is in fact a two-magnon scattering effect.

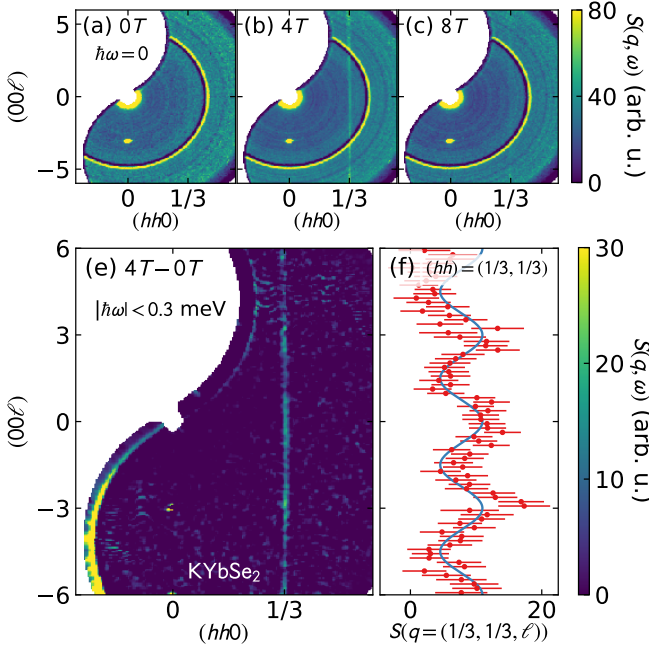


FIG. S4. KYbSe₂ elastic scattering along ℓ . Panels (a) - (c) show the elastic scattering ($\hbar\omega < 0.3$ meV) at 0 T, 4 T, and 8 T. Any elastic scattering extremely weak at 0 T and 8 T, but at 4 T a vertical streak appears at $(1/3, 1/3, \ell)$, indicating static magnetism. Panel (e) shows the 4 T with 0 T subtracted as a background, revealing a sinusoidal modulation in elastic intensity, which is plotted in panel (f) with the blue line as a guide to the eye. This evidences static magnetism in the plateau phase which is only weakly correlated between planes.

B. Nonlinear effects

For a highly quantum system like a $S = 1/2$ triangular lattice in the $1/3$ magnetization plateau phase, nonlinear corrections to magnon dispersions become significant. To illustrate this, Figure S6 shows the linear spin wave dispersions compared to the nonlinear dispersions for the best fit KYbSe₂ parameters from the main text. Particularly at low energies, the nonlinear corrections are very significant. Note that the existence of a gap (signaling a finite-field plateau phase) requires nonlinear effects to capture; this is because the plateau phase is an inherently quantum-mechanical phenomenon [S6]. Thus accurately extracting the Hamiltonian parameters from the neutron scattering measurements on KYbSe₂ requires a nonlinear spin wave model.

-
- [S1] P. J. Brown, “[Magnetic form factors](#),” The Cambridge Crystallographic Subroutine Library (1998).
 - [S2] A. Scheie, E. Ghioldi, J. Xing, J. Paddison, N. Sherman, M. Dupont, D. Abernathy, D. Pajerowski, S.-S. Zhang, L. Manuel, *et al.*, [arXiv preprint arXiv:2109.11527](#) (2021).
 - [S3] J. Xing, L. D. Sanjeewa, A. F. May, and A. S. Sefat, [APL Materials](#) **9**, 111104 (2021).
 - [S4] T. P. Robitaille, E. J. Tollerud, P. Greenfield, M. Droettboom, E. Bray, T. Aldcroft, M. Davis, A. Ginsburg, A. M. Price-Whelan, W. E. Kerzendorf, *et al.*, [Astronomy & Astrophysics](#) **558**, A33 (2013).
 - [S5] T. Xie, J. Xing, S. Nikitin, S. Nishimoto, M. Brando, P. Khannenkov, J. Sichelschmidt, L. Sanjeewa, A. S. Sefat, and A. Podlesnyak, [arXiv preprint arXiv:2106.12451](#) (2021).
 - [S6] Y. Kamiya, L. Ge, T. Hong, Y. Qiu, D. L. Quintero-Castro, Z. Lu, H. B. Cao, M. Matsuda, E. S. Choi, C. D. Batista, M. Mourigal, H. D. Zhou, and J. Ma, [Nature Communications](#) **9**, 2666 (2018).

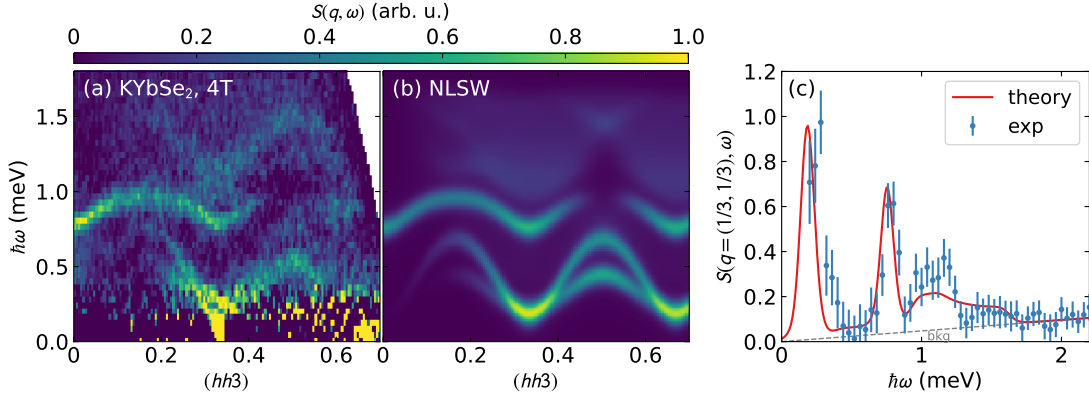


FIG. S5. Two magnon continuum of KYbSe₂. Panel (a) shows the experimental data at $B = 4$ T, and panel (b) shows the nonlinear spin wave calculated intensity with the two-magnon contribution included. Panel (c) compares the experiment with the theory at $(1/3, 1/3, 3)$. If we assume some small remnant background the overall shape and intensity of the two-magnon contribution is close to what we observe in experiment, though the calculated two-magnon intensity is slightly lower than experiment.

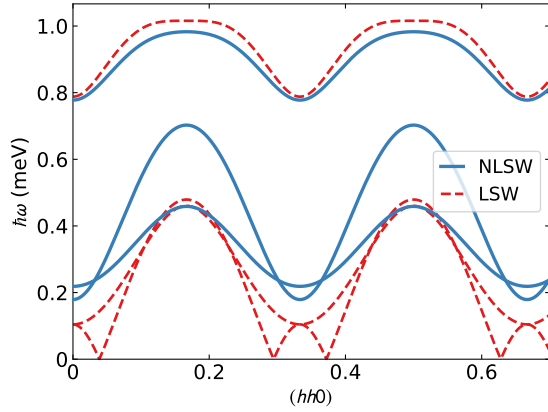


FIG. S6. Nonlinear spin wave calculations (blue) compared to linear spin wave calculations (red) for the triangular lattice using best fit parameters in the main text. Note that at this field, nonlinear corrections to the spin wave modes are significant, especially at low energies.